Biomech Model Mechanobiol (2011) 10:599–611
DOI 10.1007/s10237-010-0259-x

ORIGINAL PAPER

# Role of elastin anisotropy in structural strain energy functions of arterial tissue

**R. Rezakhaniha · E. Fonck · C. Genoud · N. Stergiopulos**

Received: 8 October 2009 / Accepted: 20 September 2010 / Published online: 7 October 2010


**Abstract** The vascular wall exhibits nonlinear anisotropic mechanical properties. The identification of a strain energy function (SEF) is the preferred method to describe its complex nonlinear elastic properties. Earlier constituent-based SEF models, where elastin is modeled as an isotropic material, failed in describing accurately the tissue response to inflation–extension loading. We hypothesized that these shortcomings are partly due to unaccounted anisotropic properties of elastin. We performed inflation–extension tests on common carotid of rabbits before and after enzymatic degradation of elastin and applied constituent-based SEFs, with both an isotropic and an anisotropic elastin part, on the experimental data. We used transmission electron microscopy (TEM) and serial block-face scanning electron microscopy (SBFSEM) to provide direct structural evidence of the assumed anisotropy. In intact arteries, the SEF including anisotropic elastin with one family of fibers in the circumferential direction fitted better the inflation–extension data than the isotropic SEF. This was supported by TEM and SBFSEM imaging, which showed interlamellar elastin fibers in the circumferential direction. In elastin-degraded arteries, both SEFs succeeded equally well in predicting anisotropic wall behavior. In elastase-treated arteries fitted with the anisotropic SEF for elastin, collagen engaged later than in intact arteries. We conclude that constituent-based models with an anisotropic elastin part characterize more accurately the mechanical properties of the arterial wall when compared to models with simply an isotropic elastin. Microstructural imaging based on electron microscopy techniques provided evidence for elastin anisotropy. Finally, the model suggests a later and less abrupt collagen engagement after elastase treatment.

**Keywords** Arterial wall biomechanics · Anisotropy · Elastin · Ultrastructure · Rabbit carotid artery · Constitutive equation

R. Rezakhaniha (✉) · E. Fonck · N. Stergiopulos
Laboratory of Hemodynamics and Cardiovascular Technology, Ecole Polytehnique Federale de Lausanne, 1015, Lausanne, Switzerland
e-mail: rana.rezakhaniha@epfl.ch

E. Fonck
e-mail: edouard.fonck@a3.epfl.ch

N. Stergiopulos
e-mail: nikolaos.stergiopulos@epfl.ch

C. Genoud
Friedrich Miescher Institute for Biomedical Research, Basel, Switzerland
e-mail: Christel.Genoud@fmi.ch

## 1 Introduction

Vascular tissue shows a nonlinear anisotropic behavior, as a result of material properties, structural arrangements and interconnections of its main constituents i.e. elastin, collagen and vascular muscle cells (Silver et al. 2003; Vito and Dixon 2003; Zhou and Fung 1997). Significant effort has been put into developing constituent-based or structural strain energy functions (SEFs) for the vascular tissue, that take into account the individual mechanical contribution of each intramural element (Driessen et al. 2005; Gasser et al. 2006; Gundiah et al. 2009; Holzapfel et al. 2000; Zulliger et al. 2004a,b) and therefore provide a solid base to study mechanical properties of the tissue in health and disease.

SEFs should provide a complete 3D description of the stress-strain field. For an axisymmetric vessel, this translates into a good description (fit) of both the pressure-radius ($P–r_o$) and the pressure-longitudinal force ($P–F_z$) curves, as those are measured in a typical inflation–extension

experiment. Most of the previously published constituent-based SEFs have considered that collagen is the only wall element contributing to the material anisotropy (Holzapfel et al. 2000; Zulliger et al. 2004a,b). Although these SEFs successfully describe P–$r_o$ curves of vessels, they fail to describe simultaneously both the P–$r_o$ and the P–$F_z$ curves, in veins (Rezakhaniha and Stergiopulos 2008) as well as in arteries (Zulliger et al. 2004a,b). In a recent study on veins, we have suggested an anisotropic SEF for elastin with fibers in the longitudinal direction, which, in conjunction with an anisotropic collagen description, significantly improved the quality of the P–$r_o$ and P–$F_z$ curves (Rezakhaniha and Stergiopulos 2008). Yet, as the anisotropy observed in the mechanical behavior of elastin could be different in arteries and veins, the present study was designed to focus on the existence and nature of elastin anisotropy in arteries. We hypothesized that a SEF with both elastin and collagen as anisotropic materials provides a better description of the mechanical properties of the arterial wall compared to traditional SEFs with anisotropic collagen and isotropic elastin components. Furthermore, we searched for direct microstructural evidence to support our hypotheses by studying the structural organization of elastin within the arterial wall. Finally, we applied our suggested SEF, with an elastin anisotropic term, to both intact and elastase-treated arteries to obtain more information about the effects of elastin fragmentation on structural links between collagen and elastin in the arterial wall.

## 2 Methods

### 2.1 Experimental data

#### *2.1.1 Biological specimens*

Six common carotids were excised from young white New Zealand rabbits ($3 \pm 0.4$ kg) from a local abattoir. The length of the arteries was measured before and after the excision to determine the in vivo longitudinal stretch of the vessels. The arteries were submerged in phosphate-buffered saline (PBS) and transported on ice to the laboratory. Immediately after arrival, the arteries were cleaned from surrounding tissue. The common carotid arteries were typically 50–60 mm in length, from which two 16-mm segments were excised. One segment was used as a control artery and the other for elastase treatment.

#### *2.1.2 Biochemical treatment*

We followed the procedure described in detail in an earlier study performed in our laboratory (Fonck et al. 2007). In summary, the artery segments were submerged in a PBS bath and stretched to their in vivo longitudinal stretch. Elastase was gradually added to the bath to reach a final concentration of 6.85 U/ml. Each artery was left in the bath for 30 min at 37°C and washed afterward with fresh PBS. To inhibit the elastase trapped in the arterial wall, the arteries were left for 30 min in a bath of 2 U/ml aprotinin (Elastin). The artery was then washed with PBS.

#### *2.1.3 Geometric measurements*

Before running inflation–extension experiments, rings of ~0.4 mm thick were cut from the end of the segments to measure the opening angle, wall thickness, and inner and outer diameter. Rings were placed in a Petri dish with PBS for 20 min at 37°C to reach an equilibrium state, and photographs were taken under an upright microscope at ×20 magnification (Axioplan2; Carl Zeiss Inc.). The rings were subsequently cut open and placed in PBS for 30 min at 37°C to measure the opening angle.

#### *2.1.4 Biomechanical testing*

Arteries were tested by an inflation–extension device described in detail in our previous study (Rezakhaniha and Stergiopulos 2008) following the protocol described by Fonck et al. (2007). In summary, the arteries were stretched to their in vivo length and then submitted to preconditioning cycles of inflation–extension (pressure range: 0–180 mmHg, approximate rate: 1.5 mmHg/s) to ensure repeatability of the curve. External diameter data was measured with a CCD micrometer (model LS-7030, Keyence). Pressure was recorded with a blood pressure transducer (BLPR, World Precision Instruments) and the longitudinal force by a load cell force transducer (FORT10, World Precision Instruments). The passive arterial state was achieved by adding sodium nitroprusside to the bath (SNP, $10^{-4}$M).

#### *2.1.5 Transmission electron microscopy*

Two intact carotid arteries were removed from the animal postmortem. These were then immersed in a solution of 2.5% glutaraldehyde and 2.0% paraformaldehyde in 0.1 M phosphate buffer, pH 7.4 for a total time of 4 h at 4°C. The arteries were initially pressurized at 70 mmHg for ten minutes, then pressure was released, and to ensure good fixation, the arteries were cut into small rings (width <3 mm). After fixation, the arteries were washed thoroughly with cacodylate buffer (0.1 M, pH 7.4), postfixed for 40 min in 1.0% osmium tetroxide, then 40 min in 5% tannic acid followed by 60 min in palladium chloride (1% in water). They were finally stained for 60 min in 1% uranyl acetate in water before being dehydrated through increasing concentrations of alcohol and then embedded in Durcupan ACM (Fluka, Switzerland) resin. The

resin was hardened for 24 h in a 65°C oven. Semi-thin sections, 1 micron thick, were cut from the trimmed blocks using glass knives to check the orientation of the vessels, and quality of the tissue, and then, thin 50-nm-thick sections were cut using a diamond knife (Diatome, Switzerland) and ultramicrotome (Leica UCT). These thin sections were further contrasted with lead citrate (Reynold's stain), and images captured digitally on a CCD camera (SIS Morada, Munich) inside a Philips CM10 transmission electron microscope at a filament voltage of 80 kV.

#### *2.1.6 Serial block-face scanning electron microscopy (SBFSEM)*

We used the same resin blocks prepared for the TEM. Image stacks were obtained using Serial block-face scanning electron microscopy SBFSEM developed by Denk and Horstmann (Denk and Horstmann 2004). The equipment is composed of a scanning electron microscope (SEM) (FEI Quanta 200 VP-FEG) combined with an ultramicrotome (3View, GATAN Inc). The ultramicrotome repeatedly removes uniform sections from the specimen surface and therefore exposes subsequent surfaces for block-face imaging by the SEM. Because the tissue block position is fixed, image registration is inherent and image distortion is absent, greatly simplifying volume reconstruction (Denk and Horstmann 2004). Images were done on three different sites in the media at the accelerating voltage of 3.5 keV and in the low vacuum mode (0.35 Torr). The section's thickness was 50 nm, and the obtained images were 2,048 × 2,048 pixels with 8.9 nm per pixel.

## 3 Mathematical model

### 3.1 Background

The mathematical model presented in this work is an extension of our work on venous tissue (Rezakhaniha and Stergiopulos 2008). We considered the artery as a thick-walled circular cylinder that undergoes inflation–extension experiments and shows a nonlinear, anisotropic and incompressible behavior. The material behavior is assumed to be pseudo-elastic i.e. loading and unloading curves can be represented by separate elastic laws as proposed by Fung (Fung et al. 1979). The principal stretch ratios are defined considering the zero stress state of the arteries, as explained in detail in our previous work (Rezakhaniha and Stergiopulos 2008). In the absence of vascular tone, we considered only passive properties of the arterial wall and therefore separated our constituent-based strain energy function into two parts representing the elastin and collagen components:

$$\Psi_{\text{passive}} = f_{\text{elast}}\Psi_{\text{elast}} + f_{\text{coll}}\Psi_{\text{coll}} \tag{1}$$

where $f_{\text{elast}}$ and $f_{\text{coll}}$ are the fractions of the wall cross-section area composed of elastin and collagen and $\Psi_{\text{passive}}$, $\Psi_{\text{elast}}$ and $\Psi_{\text{coll}}$ represent the SEF for the artery in its passive state, the SEF for the network of elastin and the SEF for the network of collagen, respectively. To be precise, $f_{\text{elast}}$ is the fraction of the wall cross-section composed of elastin that bears load, and therefore one should exclude the part of elastin area that is fragmented and thus does not bear load. Since the arteries were taken from young healthy rabbits, we have assumed that the elastin fragmentation is still low in intact arteries and that $f_{\text{elast}}$ could be assumed to be the total wall cross-section composed of elastin. As for the elastase-treated arteries, we have assumed that elastin is almost totally fragmented, and therefore $f_{\text{elast}}$ has been taken equal to 0.0. In general, the sum of the fragmented elastin and the nonfragmented elastin is equal to the total wall cross-section composed of elastin, as assessed by histology.

To define the collagen SEF, we followed the same approach as Zulliger et al. and assumed collagen as a collection of wavy fibers arranged in two helical families of fibers at angles $\alpha$ and $-\alpha$ to the circumferential direction. A detailed description of the method can be found in the study of Zulliger et al. (2004a,b). In short, the engagement of collagen fibers is assumed to take place in a statistical manner and is represented by a log logistic distribution:

$$\rho_{\text{fiber}}(E) = \begin{cases} 0 & \text{for } E \le 0 \\ \frac{k}{b}\dfrac{\left(\frac{E}{b}\right)^{k-1}}{\left[1+\left(\frac{E}{b}\right)^{k}\right]^{2}} & \text{for } E > 0 \end{cases} \tag{2}$$

$E$ is the local strain in the direction of the fiber, $b > 0$ is a scaling parameter and $k > 0$ defines the shape of the distribution. The mode (peak value) of this statistical distribution is situated at $b((k-1)/(k+1))^{1/k}$. Larger $b$ results in a later engagement, and larger scale parameter $k$ results in a more spread out distribution. However, one should be careful to compare the modeling parameters of the engagement pattern between two groups of arteries, if they have different natural zero stress states (ZSS). The reason is that, as $E$ is defined with respect to different zero stress states (ZSS), the modeling parameters will differ due to this fact alone. To be able to compare the engagement patterns, the PDFs should be defined with respect to the same reference configuration.

The strain energy function of an individual collagen fiber is defined by:

$$\Psi_{\text{fiber}}(E) = \begin{cases} 0 & \text{for } E \le 0 \\ c_{\text{coll}}\frac{1}{2}E^2 & \text{for } E > 0 \end{cases} \tag{3}$$

where $c_{\text{coll}}$ is an elastic constant associated with collagen fibers. The contribution of the ensemble of collagen fibers to

the SEF is therefore given by:

$$\Psi^{f}_{\text{coll}}(E) = \Psi_{\text{fiber}} * \rho_{\text{fiber}} = \int_{-\infty}^{\infty} \rho_{\text{fiber}}(E^*)\Psi_{\text{fiber}}(E - E^*)dE^* \quad (4)$$

where $\Psi^{f}_{\text{coll}}$ is the strain energy function for the ensemble of the fibers. Assuming that collagen fibers are at an angle $\alpha$ to the circumferential direction in the $e_\theta$–$e_z$ plane and their direction is represented by the unit vector $v_\alpha$, we can define $I_4$, an invariant of the Cauchy-Green tensor $\boldsymbol{C}$ with respect to $v_\alpha$, as :

$$I_4 = v_\alpha \cdot \boldsymbol{C} \cdot v_\alpha = \lambda^2 = \lambda_\theta^2 \cos^2\alpha + \lambda_z^2 \sin^2\alpha \quad (5)$$

Similarly, we can define the invariant $I_4^{'}$ with respect to a vector $v_\alpha^{'}$ having the angle $-\alpha$ with the circumferential direction. As we assumed that fibers are organized symmetrically around the longitudinal direction, $I_4^{'}$ and $I_4$ are equal in this case.

Thus, the collagen SEF, with half of the fibers at angle $\alpha$ and the other half at $-\alpha$ to the circumferential direction, becomes:

$$\Psi_{\text{coll}} = f_{\text{coll}}\left(\frac{1}{2}\Psi^{f}_{\text{coll}}\left(\frac{I_4 - 1}{2}\right) + \frac{1}{2}\Psi^{f}_{\text{coll}}\left(\frac{I_4' - 1}{2}\right)\right) \quad (6)$$

#### *3.1.1 Anisotropic strain energy function for elastin*

To define the SEF for elastin, we propose a combination of an orthotropic model, accounting for a subset of elastin fibers oriented in the circumferential direction and an isotropic model, accounting for the remaining elastin matrix:

$$\Psi_{\text{elast}} = \Psi_{\text{iso}}(I_1) + \Psi_{\text{aniso}}(I_4'') \quad (7)$$

where $I_1$ is the first invariant of the Cauchy–Green deformation tensor $\boldsymbol{C}$ and $I_4''$ is an invariant of $\boldsymbol{C}$ with respect to the $e_\theta$ defined as:

$$I_4'' = e_\theta \cdot \boldsymbol{C} \cdot e_\theta = \lambda_\theta^2 \quad (8)$$

$e_\theta$ is the unit vector in the circumferential direction.

For the isotropic component of elastin, we used a neo-Hookean SEF:

$$\Psi_{\text{iso}} = c^{i}_{\text{elast}}(I_1 - 3) \quad (9)$$

where $c^{i}_{\text{elast}}$ represents the modulus for the isotropic elastin component. As for the anisotropic component, we assumed the one-dimensional form of an incompressible neo-Hookean material for each fiber, undergoing a uniform cross-section deformation when stretched in the fiber direction. This results in the following formulation for the anisotropic part of the SEF:

$$\Psi_{\text{aniso}} = c^{a}_{\text{elast}}\left(I_4'' + \frac{2}{\sqrt{I_4''}} - 3\right) \quad (10)$$

where $c^{a}_{\text{elast}} > 0$ is an elastic constant enabling us to obtain a higher modulus for elastin in the circumferential direction.

Combining the individual SEF for collagen and elastin, we obtain the global SEF of the artery at its passive (no vascular tone) state as:

$$\Psi_{\text{passive}} = f_{\text{elast}}\left(c^{i}_{\text{elast}}(I_1 - 3) + c^{a}_{\text{elast}}\left(I_4'' + \frac{2}{\sqrt{I_4''}} - 3\right)\right) + f_{\text{coll}}\left(\frac{1}{2}\Psi_{\text{coll}}\left(\frac{I_4 - 1}{2}\right) + \frac{1}{2}\Psi_{\text{coll}}\left(\frac{I_4' - 1}{2}\right)\right) \quad (11)$$

### 3.2 Comparing patterns of collagen engagement

The natural ZSS of the control arteries is different from the elastase-treated arteries. Therefore, the modeling parameters related to the Eq. 2 cannot be directly used to compare the pattern of collagen engagement. In order to compare collagen engagement characteristics, the probability density functions of the control and the elastase-treated arteries should be presented with respect to the same reference configuration.

If $E^c$ and $E^t$ are green strains along the fibers, with respect to the ZSS of control and treated arteries, respectively, and $\rho^c$ $(E^c)$ and $\rho^t$ $(E^t)$ are the corresponding PDFs,

$$\int_{-\infty}^{\infty} \rho^c(E^c)dE^c = \int_{-\infty}^{\infty} \rho^t(E^t)dE^t = 1 \quad (12)$$

If the function of $E^c$ versus $E^t$ is monotonic, the above equation results in,

$$\rho^c(E^c)dE^c = \rho^t(E^t)dE^t \quad (13)$$

To calculate the relation between $E^c$ and $E^t$, first, we have assumed that a point on the wall of the control group is linearly transformed to a point on the wall of the elastase-treated arteries. For instance, a point on the midline of a control artery would be transformed to a corresponding point on the midline of the treated one. Second, the changes in the reference configuration, i.e the changes in the OA, the radii and the length after elastase treatment have been taken into account to calculate the relation between $E^c$ and $E^t$. Finally, we have assumed that the relation between $E^c$ and $E^t$ for a point on the midline could represent the mean transformation for the whole arterial wall. In the range of applied deformations, this assumption results in a maximum error of 14% in calculations of $E^t$ based on $E^c$.

### 3.3 Fit function

Pressure-radius and pressure-longitudinal force curves were fitted to the experimental data by minimizing the following function:

$$\Phi = \frac{1}{2}\frac{1}{m}\sum_{i}^{m}\left(\frac{r_i^{\mathrm{mod}} - r_i^{\mathrm{exp}}}{\sigma_i^r}\right)^2 + \frac{1}{2}\frac{1}{m}\sum_{i}^{m}\left(\frac{F_i^{\mathrm{mod}} - F_i^{\mathrm{exp}}}{\sigma_i^F}\right)^2 \tag{14}$$

$m$ is the number of experimental points measured at different pressures. Superscript *mod* denotes the values predicted by the mathematical model, whereas superscript *exp* those measured experimentally. The index $i$ denotes the pressure at which the corresponding outer radius, $r$, and the longitudinal force, $F$, were obtained. $\sigma$ is the standard deviation of the experimental mean value of radius or force at a given pressure and longitudinal stretch ratio. It is used as a weighting factor, giving more weight to the points with the least variation.

In order to check the fit quality, the weighted residual sum of squares for radius and force, $WRSS^r$, $WRSS^F$, have been calculated based on the following formula:

$$WRSS^k = \sum_{i}^{m}\left(\frac{k_i^{\mathrm{mod}} - k_i^{\mathrm{exp}}}{\sigma_i^k}\right)^2 \qquad k = r, F \tag{15}$$

## 4 Results

$P–r_o$ and $P–F_z$ curves from inflation–extension experiments on intact arteries and elastase-treated arteries are plotted in Fig. 1. As seen from the $P–r_o$ curves, the vessel inflates more abruptly at lower pressures in elastase-treated arteries than the intact arteries and the final diameter reached at 20 kPa is higher in elastase-treated arteries (1.76 mm) than intact arteries (1.46 mm). In addition, based on $P–F_z$ curves, the elastin degradation causes a decrease in the measured longitudinal force in low pressures (between 0 and 10 kPa) and at higher pressures, makes the curve less steep. Elastase treatment led to a 24, 9 and 27% increase in the external diameter, internal diameter and the axial length in the zero load configurations, respectively. The opening angle was substantially decreased from 107 ± 24 degrees in intact arteries to 11.5 ± 8.4 degrees in elastase-treated arteries.

Figure 2 shows the $P–r_o$ and $P–F_z$ curve fits based on the original model, with an isotropic elastin term. Column (a) presents the fit from original Zulliger et al. model, when only the $P–r_o$ curve was considered to fit the data and no importance was given to the $P–F_z$ curve in the fitting process. In this case, the model closely fits the $P–r_o$ curve ($WRSS^r = 3.72$), yet gave a relatively poor fit for the $P–F_z$ curve ($WRSS^F =$ 643). When the $P–r_o$ and $P–F_z$ curves were both considered in the fitting process, i.e. function $\Phi$ was optimized, this resulted in $\Phi = 1.189$, and the fit is shown in column (b). The quality of the fit for the $P–F_z$ curve was improved, and $WRSS^F$ was reduced to 55.26 at the expense of the quality of the $P–r_o$ fit ($WRSS^r = 23.23$).

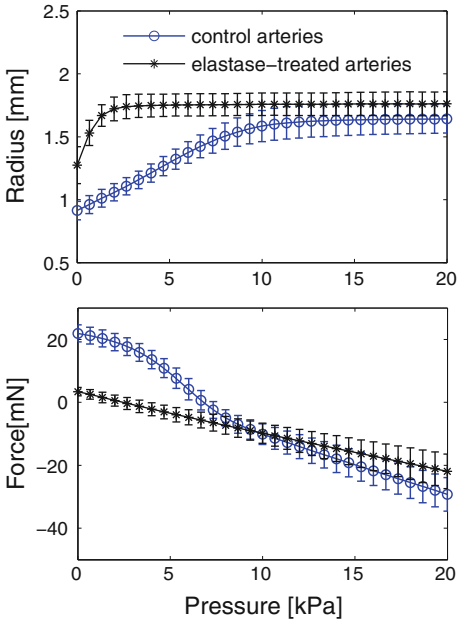


**Fig. 1** Experimental data from control and elastase-treated arteries

Figure 3 presents the fits of the modified model with an anisotropic elastin component applied on the experimental data of intact arteries. The fit was considerably improved compared to the one resulted from the original model with an isotropic elastin ($WRSS^r = 3.65$, $WRSS^F = 9.04$ for the modified model compared to $WRSS^r = 23.23$, $WRSS^F = 55.26$ in the original model). The fit function $\Phi$ was reduced to 0.1909 compared to 1.189 from the best fit of the original model (Fig. 1b).

The parameters used in minimizing $\Phi$ in the fit procedure are listed in Table 1 for the original model with isotropic elastin component and the modified model with an anisotropic elastin component having fibers in the $\theta$-direction. The model resulted in $WRSS^r = 157$ and $WRSS^F = 8,377$ when the same parameters as for the best fit of the modified model from Table 1 were applied on the experimental data of elastase-treated arteries (Fig. 4a). To improve the quality of the fit, $b$ and $\alpha$ were let free to change, while other parameters were held constant which resulted in $b = 0.832$ and $\alpha = 0.80$ rad compared to the original values of $b = 1.63$ and $\alpha = 0.68$ rad. The result of the new fit is plotted in Fig. 3b ($WRSS^r = 7.85$ and $WRSS^F = 32.23$), and the parameters used are indicated in Table 2.

The probability density function of the log logistic distributions assumed for collagen engagement is plotted in Fig. 5.

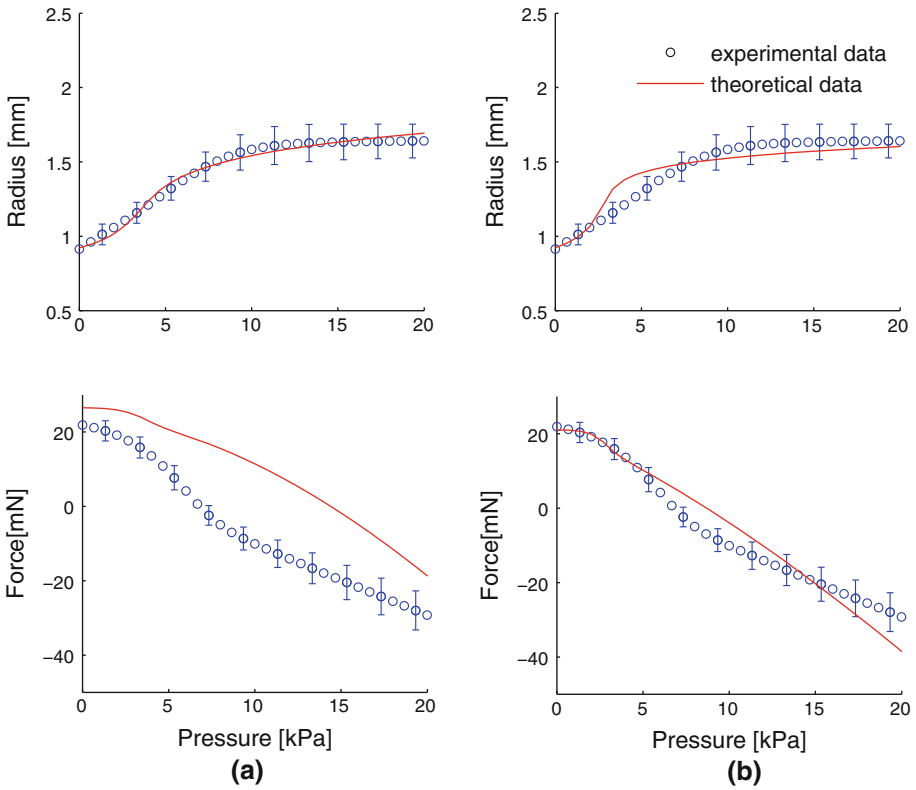


**Fig. 2** Original model of Zulliger et al., with an isotropic term for elastin, applied on intact arteries a) when only P–$r_o$ is fitted and b) when both P–$r_o$ and P–$F_z$ are fitted

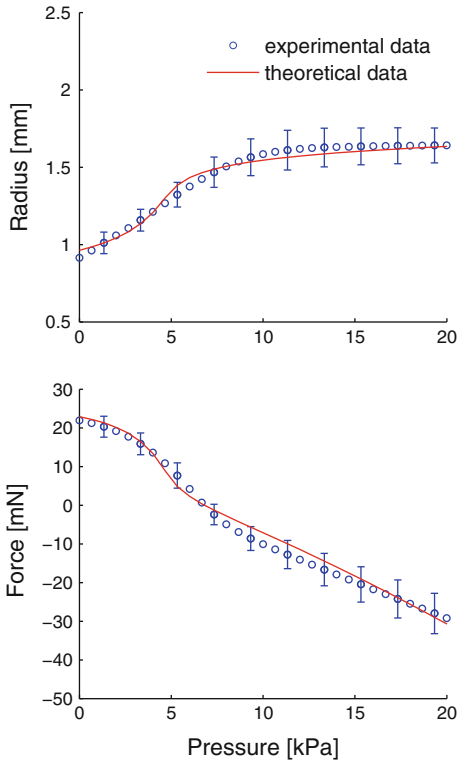


**Fig. 3** Modified model of Zulliger et al., with an anisotropic SEF for elastin, applied on intact arteries when both P–$r_o$ and P–$F_z$ are fitted

Figure 5a and b shows the distribution for two sets of parameters from Table 2, as assessed by the fitting of the model; first, $k = 6.64$ and $b = 1.63$ (parameters related to the best fit on the data of intact arteries) and second, $k = 6.64$ and $b = 0.832$ (related to the best fit of elastase-treated arteries). To compare the engagement pattern of collagen, Fig. 5c plots the resulted distributions from Fig. 5a and b with respect to the same reference configuration (elastase-treated group). The transformation has been obtained using Eq. 13 and considering the changes in the geometry of the ZSS configuration after elastase treatment. As seen from Fig. 5c, in elastase-treated arteries, collagen engages at higher values of strain compared to intact arteries. The collagen engagement is less abrupt. The distribution is extended between $E^t = 0.2$ and

**Table 1** Parameters used in minimizing $\Phi$ in intact arteries

| Strain energy function | Original model (with isotropic elastin) | Modified model (with anisotropic elastin) |
|---|---|---|
| Fitted parameters | $c^i_{\text{elast}} = 17.99\,\text{KPa}$ | $c^i_{\text{elast}} = 18.39\,\text{KPa}$ |
| | | $c^a_{\text{elast}} = 13.59\,\text{KPa}$ |
| | $k = 5.35$ | $k = 6.64$ |
| | $b = 1.96$ | $b = 1.63$ |
| | $\alpha = 0.60\,\text{rad}$ | $\alpha = 0.68\,\text{rad}$ |
| Experimentally defined parameters | $f_{\text{elast}} = 0.3$ | $f_{\text{elast}} = 0.3$ |
| | $f_{\text{coll}} = 0.3$ | $f_{\text{coll}} = 0.3$ |
| Imposed on model | $c_{\text{coll}} = 200\,\text{MPa}$ | $c_{\text{coll}} = 200\,\text{MPa}$ |
| $\Phi$ | 1.189 | 0.1909 |

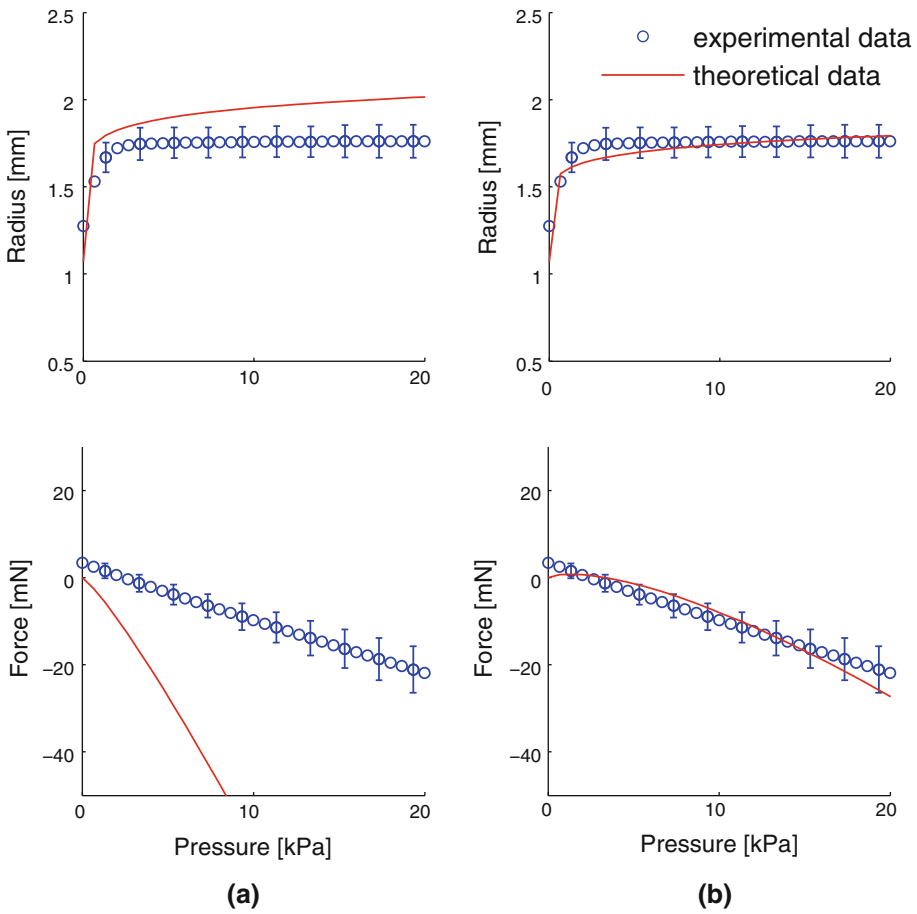


**Fig. 4** Modified model of Zulliger et al., with an anisotropic term for elastin, applied on elastase-treated arteries (**a**) with same parameters as optimized for the intact arteries (based on Table 1) and (**b**) when parameters $b$ and $\alpha$ are optimized

2, while in intact arteries, collagen engages between $E^t = 0$ and 0.6.

Figure 6 shows a TEM image of the arterial cross-section in the media. Elastin, smooth muscle cells and collagen fibers are depicted in dark, medium and light gray, respectively. In the arterial cross-sections, interlamellar elastin fibers (arrows) made links between elastin lamina (asterisks) and SMCs and were oriented in the similar direction as the SMCs. Figure 7 indicates a 2D SBFSEM image of the arterial cross-section where the same pattern was observed but with the elastin in light gray and collagen in dark gray. Figure 8 illustrates an example of 3D SBFSEM images. An intralamellar elastin feature is marked with arrows in the image. In Fig. 9, one could follow the same IEF structure in 3D by choosing proper planes of views. As seen from the planes A and B, the IEF runs obliquely in the $\theta$-r plane making a slight angle (around 2.5°) with the lamellar elastin (i.e. circumferential direction) and does not extend in the z-direction. In addition, 3D SBFSEM images were examined in three different sites. IEFs appeared mainly in the circumferential direction in all layers; however, they became less organized when located in layers closer to the intima compared to those closer to the adventitia. Moreover, moving from the intima to the adventitia, IEFs became more abundant and thicker in diameter.

**Table 2** Parameters used in Fig. 3 for elastase-treated arteries

| | Parameters from the best fit of intact arteries | $K$ and $\alpha$ optimized for elastase-treated arteries |
|---|---|---|
| Fixed parameters | $c^i_{\text{elast}} = 18.39\,\text{KPa}$ | $c^i_{\text{elast}} = 18.39\,\text{KPa}$ |
| | $c^a_{\text{elast}} = 13.59\,\text{KPa}$ | $c^a_{\text{elast}} = 13.59\,\text{KPa}$ |
| | $c_{\text{coll}} = 200\,\text{MPa}$ | $c_{\text{coll}} = 200\,\text{MPa}$ |
| | $k = 6.64$ | $k = 6.64$ |
| | $b = 1.63$ | |
| | $\alpha = 0.68\,\text{rad}$ | |
| Free parameters | $f_{\text{elast}} = 0.0$ | $f_{\text{elast}} = 0.0$ |
| | $f_{\text{coll}} = 0.3$ | $f_{\text{coll}} = 0.3$ |
| | No optimization | $b = 0.832$ |
| | | $\alpha = 0.80\,\text{rad}$ |
| $\Phi$ | 129.1 | 0.456 |

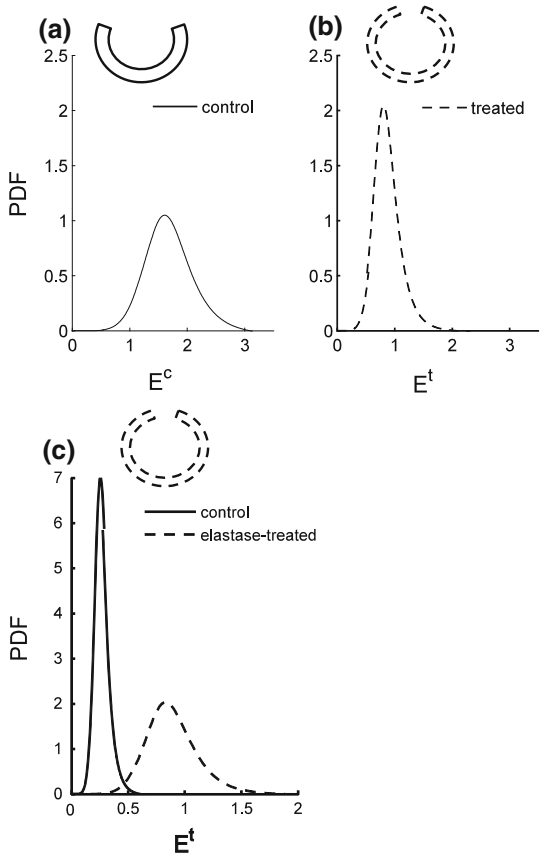


**Fig. 5** Probability density functions of the log logistic collagen distribution related to **a** the control group with respect to the control arteries' reference geometry (model parameters $k = 6.64$, $b = 1.63$, as fitted to the control group), **b** the elastase-treated group with respect to the treated reference geometry (model parameters $k = 6.64$, $b = 0.832$, as fitted to the elastase-treated group and **c** the control group (*solid line*) and elastase-treated group (*dashed line*) with respect to the elastase-treated reference geometry

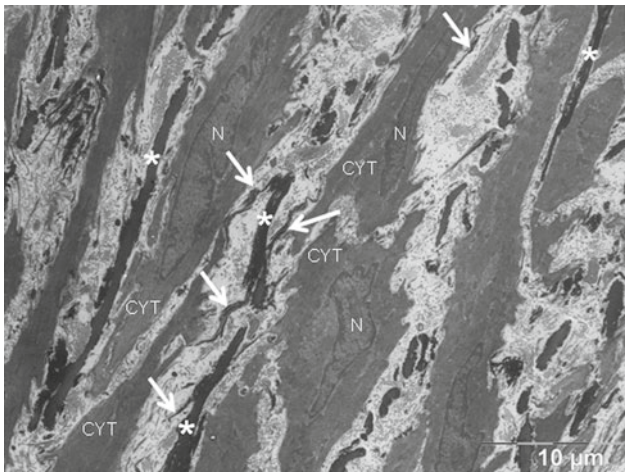


**Fig. 6** A TEM image of the arterial cross-section showing SMC's nucleus ($N$) and cytoplasm ($CYT$), elastin laminas ($asterisks$) and intralamellar elastin fibers ($arrows$)

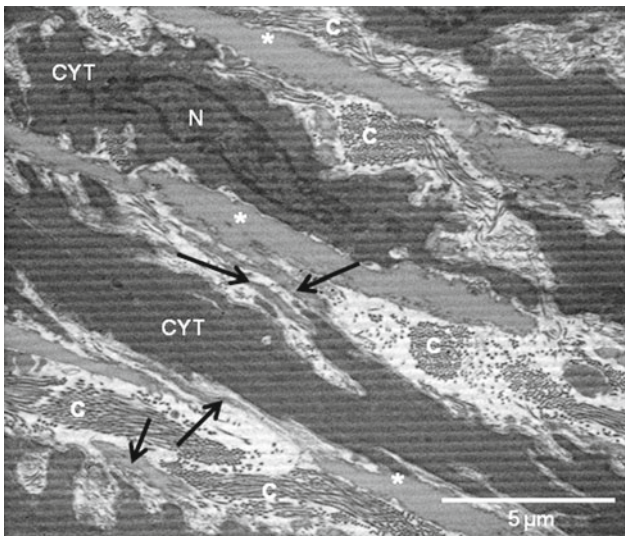


**Fig. 7** A 2D SBFSEM image of arterial cross-section showing SMC's nucleus ($N$) and cytoplasm ($CYT$), collagen fibers ($C$), elastin laminas ($asterisks$) and intralamellar elastin fibers ($arrows$)

## 5 Discussion

Our results showed that including an anisotropic formulation for the SEF of elastin, with one family of fibers in the circumferential direction, could significantly improve the quality of P–$r_o$ and P–$F_z$ curve fits ($\Phi$ value was reduced from 1.189 to 0.1909). Assessment of arterial tissue ultrastructure, based on scanning microscopy techniques, revealed interlamellar elastin fibers running in the circumferential direction between the elastin lamellar sheets, thereby providing substantial evidence for this anisotropy. These ultrastructural features were formulated in an anisotropic strain energy function for elastin, which included an isotropic part, representing the elastin lamellar sheets, and an anisotropic part for the family of fibers in the circumferential direction. The results also indicated that in the absence of a structurally functional elastin, collagen engages less abruptly and the angle of collagen fibers is altered.

### 5.1 Elastin in constituent-based SEFs

In the present study, we have suggested a transversely isotropic SEF for arterial elastin with elastin as a fiber-reinforced material having one family of fibers in the circumferential direction. Table 3 summarizes characteristics of some constituent-based SEFs previously reported in the literature. The table provides the properties of each mural constituent considered for the formulation of the SEF and the type of the experimental data used to validate these SEFs. In both the SEF of Holzapfel et al. (2000) and the model of Zulliger et al. (2004a,b), collagen is the only constituent that contributes to the anisotropic properties of the vascular tissue, and elastin is considered as an isotropic material. These models

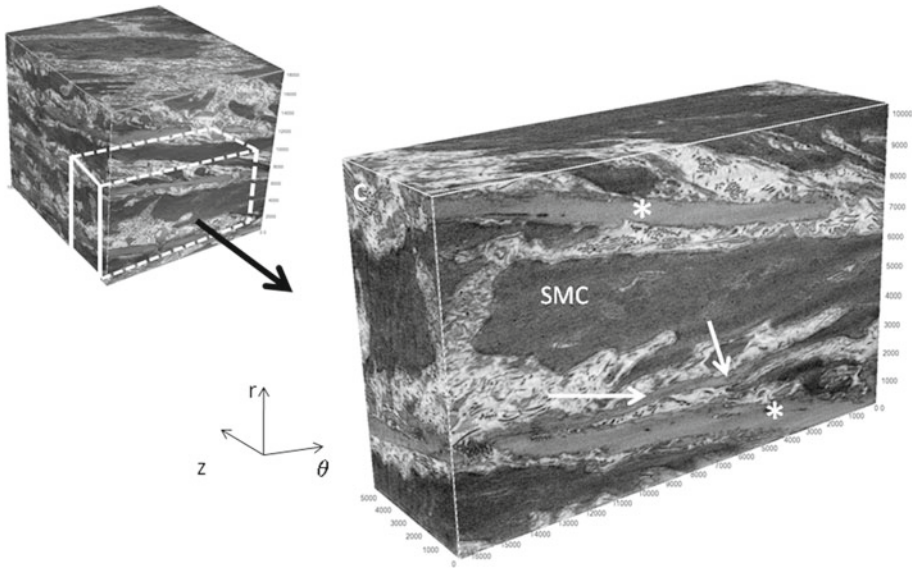


**Fig. 8** 3D SFBSEM images showing an arterial volume: IEFs (*arrows*) and Elastin lamella (*asterisks*) can be seen on the images. IEFs run obliquely, spread from elastic lamella and end in SMCs. Volume dimensions are 18 μm, 10 μm and 5 μm

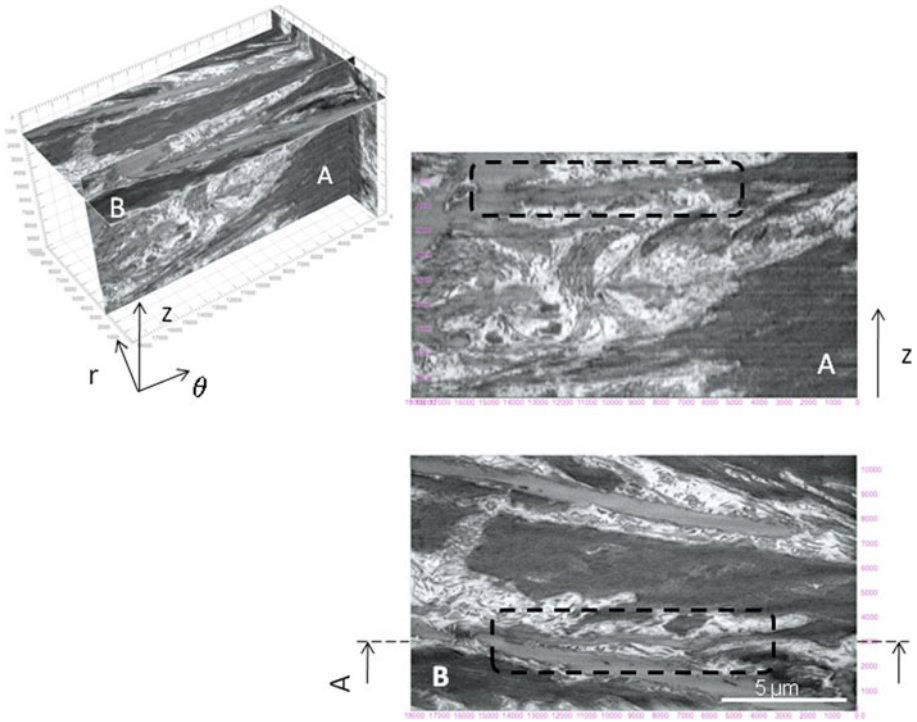


**Fig. 9** An interlaminal elastin structure as seen by 3D SFBSEM images. The intersection of *planes A and B* have been chosen on an IEF structure. The IEF does not extend in *z* direction and is almost parallel with elastin laminae thus in the circumferential direction

were validated using P–$r_o$ curves of intact arteries. However, when forced to fit the P–$r_o$ and P–$F_z$ curves simultaneously, they provided a poor fit (Rezakhaniha and Stergiopulos 2008; Zulliger et al. 2004a,b). Our results suggest that the shortcomings of these models to fit the multidimensional data are, at least partly, due to the elastin definition in their constituent-based SEF. The collagen term in their SEF seems to be appropriate, because it can successfully fit both the P–$r_o$ and the P–$F_z$ curves simultaneously in the absence of elastin (Fig. 4b). However, including other structural features could also play a role in improving the quality of the fit. Among these features, one could mention the dispersion of the fibers or the multilayered structure of the arterial wall.

The present study indicates that an anisotropic formulation for elastin can improve the match between SEF and experimental measurements. In a former study on isolated arterial elastin (autoclaved and alkali treated), Gundiah and colleagues tested pig thoracic aortas using a biaxial stretcher system. They proposed an orthotropic material symmetry for arterial elastin, but suggested that an isotropic SEF could successfully describe the biaxial data (Gundiah et al. 2007, 2009). Since the microstructure and mechanical behavior of

**Table 3** A summary of existing constituent-based SEFs

| | Experimental data used for validation | Elastin | Collagen | SMCs |
|---|---|---|---|---|
| Holzapfel et al. (2000) | Various intact arteries | Isotropic | Anisotropic<br>Two family of fibers<br>Orientation of fibers | – |
| Zulliger et al. (2004a,b) | Various intact arteries | Isotropic | Anisotropic<br>Two family of fibers<br>Orientation of fibers<br>Waviness of fibers | Contraction state |
| Gundiah et al. (2007) | Autoclaved and alkali-extracted porcine thoracic arteries | Isotropic (two orthogonal family of fibers with same material properties) | – | – |
| Rezakhaniha and Stergiopulos (2008) | Intact rabbit facial veins | Anisotropic (one family of fibers in the longitudinal direction) | Anisotropic<br>Two family of fibers<br>Orientation of fibers<br>Waviness of fibers | – |

normal arterial wall varies with location along the vascular tree and species (Humphery 2002), the observed difference in mechanical behavior of elastin could be species/location dependent (pig thoracic aorta vs rabbit common carotid). In addition, the study of Gundiah et al. was based on techniques of collagen digestion. Digestion techniques can affect the mechanical properties of the resulting network. For example, hot alkali treatment causes fragmentation of the elastin network (Daamen et al. 2001; Lillie and Gosline 1990). Finer features, such as IEFs, might also be degraded, while larger features remain. The damage in fine structures could affect the degree of elastin anisotropy, but this needs to be verified through careful ultrastructural assessment with appropriate imaging techniques.

In a recent study on rabbit facial veins, we have suggested an anisotropic SEF considering elastin as a fiber reinforced material with one family of fibers in the longitudinal direction (Rezakhaniha and Stergiopulos 2008). In the current study on arteries, we observed likewise that an anisotropic formulation for elastin could improve the quality of fits. However, contrary to the longitudinal orientation of elastin fibers in veins, we had to consider the fibers in the circumferential direction to obtain the best fit in arteries. In the present study, the circumferential direction of fibers was justified by the circumferential direction of IEF structures in arteries (Fig. 9). In the study on veins, no histological reason for fiber direction was investigated and the results were only based on the quality of the fits. Assuming that the direction of IEFs dictates the direction of fibers in the SEF, one can imagine axially oriented IEFs for the studied veins. A more detailed study of elastin structure in veins and arteries could be helpful to clarify the subject.

The present model assumes that all elastin fibers are oriented in the circumferential direction. This assumption is supported by the visual inspection of microscopic images of the wall structure. Yet, realistically, the fibers are distributed around some mean direction. Consequently, the dispersion of fiber orientation could influence the overall behavior of the model. Based on our results, the model with only one family of fibers in the circumferential direction could fit successfully the experimental data. Therefore, we believe that considering all the fibers in an effective circumferential direction is an acceptable assumption. A detailed future study on the angular distribution of IEFs would be needed to validate our assumption and to define in greater detail the structural properties of the elastin fiber network.

As for the isotropic part of elastin, we have chosen a neo-Hookean SEF, suggested by Holzapfel and Weizsacker (Holzapfel and Weizsacker 1998). This was different from our previous study on veins (Rezakhaniha and Stergiopulos 2008) where the SEF suggested by Zulliger et al. was utilized (Zulliger et al. 2004a,b):

$$\Psi_{\text{iso}} = c^{i}_{\text{elast}}(I_1 - 3)^{3/2} \tag{16}$$

The model by Zulliger et al. was based on an improved fit to the gross mechanical response of arteries. Watton et al. recently compared the model of Zulliger et al. for elastin with the neo-Hookean model and concluded that the neo-Hookean model captures more accurately the mechanical response of elastin (Watton et al. 2009). In summary, they observed

that the model suggested by Zulliger et al. does not yield a good fit to (uniaxial) experimental data within the physiological range of stretches. Furthermore, the infinitesimal shear modulus is zero in the linear limit and therefore, violating a basic requirement of continuum mechanics. Finally, the SEF is not well defined for $I_1 - 3 < 0$, i.e. if the material is slightly compressible. Therefore, the Zulliger et al. SEF may give rise to numerical difficulties in finite element applications. If, on the other hand, elastin is modeled as a rubber-like material, the neo-Hookean formulation has a sound theoretical basis (Treloar 1942).

### 5.2 Elastin 3D ultrastructure in arteries

By definition, constituent-based SEFs need to contain the structural information of each constituent. In this study, we tried to explain the suggested form of the elastin anisotropy based on its 3D structure. The 3D structure of arterial elastin has been subject to some controversial studies. While in some species, including man, the individual fibers appear to coalesce to form continuous, uninterrupted sheets, other studies in the pig aorta indicate that the medial elastic fibers retain their individuality and do not form sheets (Clark and Glagov 1985; Grut et al. 1977). Most of these previous microstructural studies have used the information from 2D views in which complex features can easily be misinterpreted. Recently, Denk and Colleagues developed a new technique called the serial block-face scanning electron microscopy (SBFSEM) to produce nanostructural information in three dimensions (Briggman and Denk 2006; Denk and Horstmann 2004). O'Connell et al. used this novel technique to obtain 3D volumetric information of aortic medial microstructure and described in detail the 3D organization of each wall element in rat abdominal aorta (O'Connell et al. 2008). In the present study, we have used SBFSEM as well as transmission electron microscopy (TEM) to access the structural organization of elastin in arteries. These techniques provide a basis to define the form of the suggested anisotropic SEF for arterial elastin.

In our study, TEM and SBFSEM images suggested a nearly circumferential direction of interlamellar elastin fibers. Using TEM, we observed elastin fibers going from lamella to SMCs in a nearly circumferential direction between elastin sheets. These structures were not found in transversely cut sections and we could only detect a cross-sectional view of elastin fibers, suggesting that interlamellar elastin structures do not continue in the longitudinal plane and are limited to the circumferential–radial plane. This was confirmed by the 3D SBFSEM images (Fig. 9). These results constitute the structural basis for the suggested anisotropic form of the arterial elastin, derived from the family of fibers in the circumferential directions.

Our results are in accordance with earlier ultrastructural studies of arteries (Clark and Glagov 1979, 1985; Dingemans et al. 2000; O'Connell et al. 2008). Specifically, in a recent study, O'Connell et al. described in detail the medial ultrastructure of rat abdominal aorta using SBF-SEM and confocal microscopy techniques. They reported three unique forms of elastin in the aorta i.e. lamellae, IEFs and radial elastin struts. Of the total elastin volume, lamellae comprised 71%, IEFs 27% and radial elastin struts the remaining 2%. Similar to the current study, O'Connell and colleagues reported that IEFs and SMC nuclei were preferentially oriented in the circumferential direction, which is in agreement with our findings.

### 5.3 Collagen's engagement pattern and angle in absence of elastin

To study interlinks between collagen and elastin structures, we have applied our suggested SEF on the experimental data from intact and elastin-degraded arteries. Experimental data from vascular tissues, where selectively one of the wall constituents is altered, could be useful in assessing the material behavior of each constituent, their functional coupling and interlinks between different wall elements. These data are therefore helpful to develop the SEF of different wall constituents. Among models with selectively altered constituents, elastase-treated arteries offer an attractive model to access the biomechanical properties of arteries after elastin degradation, as seen in pathologies such as aortic stiffening with age and aneurysm formation (Dobrin 1989; Dobrin and Canfield 1984; Hayashi et al. 1987). Recently, Fonck et al. studied the collagen engagement profile in intact and elastase-treated arteries by applying the SEF proposed by Zulliger et al. on $P–r_o$ curves and suggested a clear interaction between collagen and elastin in the arterial wall (Fonck et al. 2007). Following the same approach, in the present study, we extended the work of Fonck et al., first by using both $P–r_o$ and $P–F_z$ curves from intact and elastase-treated arteries and second by applying the newly proposed SEF including the elastin anisotropic term.

The values reported for $k$ and $b$ by Fonck et al. are different from the current study (Fonck et al. 2007). Fonck et al. suggested peak values of collagen distributions at $E = 0.912$ in control arteries and 0.869 in elastase-treated arteries compared to the corresponding 1.557 and 0.794 in the current study. Fonck et al. assumed a circumferential direction for collagen fibers and used only $P–r_o$ curves to fit the data. On the contrary, we let free the angle of collagen fibers, which was necessary to fit simultaneously both $P–r_o$ and $P–F_z$ curves. The choice of angle of collagen fibers may have led to different values of $k$ and $b$ in these studies. More importantly, we used a neo-Hookean SEF ($I_1 - 3$) as the isotropic term for elastin. Fonck et al. applied a different SEF suggested by

Zulliger et al. ($(I_1 - 3)^{3/2}$) which makes the elastin stiffer at higher strains and therefore alters the engagement parameters of collagen.

In addition, Fonck et al. tried to compare the engagement pattern of collagen fibers between control and elastase-treated groups and suggested a more abrupt and earlier engagement pattern for collagen after elastase treatment. This was achieved by comparing directly the fitted parameters and the corresponding distributions. However, since the natural reference configuration of the control and elastase-treated arteries is different, the comparison of distributions is not straightforward. The PDF related to the control group (Fig. 5a) is a function of the Green strain with respect to the ZSS of the control group ($E^c$), while the PDF related to the treated groups (Fig. 5b) is a function of the Green strain with respect the ZSS of the treated group ($E^t$). Therefore, if the PDFs are compared directly, the changes in the shape of the distribution could be merely because of the differences in the ZSSs. In order to compare the collagen engagement pattern, the PDFs should be represented as a function of the same Green strain (Fig. 5c). This can be achieved by using Eq. 13, once the relation between $E^t$ and $E^c$ is known.

To calculate the relation between $E^t$ and $E^c$, we have assumed that the transformation for a point on the midline could represent the mean transformation law for the whole arterial wall. Let us consider a collagen fiber at the mid wall of a control artery, with an angle of 39° to the circumferential direction. After elastase treatment, this fiber is subjected to an elongation of 156% as a result of (a) the diameter expansion of 15%, (b) the axial elongation of 27% and (c) the OA decrease of 240% (from 107° to 31°). This results in the transformation of the PDF in Fig. 5a into Fig. 5c (solid line).

Figure 5c could be therefore used to elucidate the effect of elastase treatment on the collagen engagement pattern. The elastase treatment seems to result in a later and less abrupt engagement of collagen fibers compared to the control group. This may suggest possible structural links between collagen and elastin which are altered after elastase treatment, resulting in a wavier structure and therefore a later and less abrupt engagement pattern. Further studies are needed to elucidate the role of geometrical changes and possible mechanical interactions between collagen and elastin following the elastin degradation.

As for the modification in the effective angle of collagen fibers ($\alpha$), based on Table 2, the angle was increased by 18% after degradation of elastin. Only by letting free $\alpha$, we could fit both the P–$r_o$ and P–$F_z$ curves simultaneously in both intact and elastase-degraded arteries. We reported an angle of 0.68 rad (39°) for collagen fibers in intact arteries. Holzapfel et al. have chosen an angle of 29° in their original model (Holzapfel et al. 2000), Driessen et al. have taken $\alpha = 30°$ for the media layer (Driessen et al. 2005). Zulliger et al. found this angle to be 35.0° in porcine carotid arteries (Zulliger et al. 2004a,b). Thus, the angle obtained in the present study is close to previously reported values.

### 5.4 Limitations

The vascular smooth muscle (VSM) plays an important role in the mechanical properties of the arterial wall. We have neglected the contribution of VSM, because we intended to look only at the "passive" components of the wall, which are principally elastin and collagen and to do so we tested arteries under maximally dilated vascular smooth muscle (VSM). This was achieved in our study by adding a high dose of sodium Nitroprusside, which according to earlier studies and literature guarantees maximal vasodilation. Maximally dilated VSM is assumed to have a negligible effect on mechanical properties of elastic arteries at its passive state. The assumption has been on the basis that its passive elastic modulus is reported to be about one order of magnitude less than that of elastin (VanDijk et al. 1984). We acknowledge the potential shortcoming of our model, which derives from the fact that other wall components (proteoglycans, ground substance, etc.) were also assumed to have a negligible mechanical effect when compared to the principal structural components, i.e. elastin and collagen. However, one could assume that the neo-Hookean model not only accounts for the isotropic part of elastin, but also includes other wall components.

Electron microscopy images show that smooth muscle cells are oriented in the same direction as Interlamellar elastin fibers (IEFs) and thus could contribute to the mechanical properties in the same direction as IEFs. Therefore, the fact that we attribute anisotropy of elastin solely to IEF may not be entirely true and anisotropy at low strains could be also the result of the combined effect of the in-series ensemble of IEF and VSM. Earlier experimental (Roy et al. 2005) and theoretical work (Roy et al. 2005) from our laboratory points toward this direction.

The model suggested in this study is a one-layer model, and structural properties have been homogenized throughout the arterial wall. Clearly, this does not reflect reality, knowing that the adventitia is primarily comprised of collagen. However, the artery considered in this study (rabbit common carotid) is an elastic artery with the adventitia occupying only about 10% of the wall. Therefore, although a two-layer model could more correctly capture the structural properties of the rabbit common carotid, the error of using a one-layer model may be not so significant. Of course, even within the media alone, we have a multilayer structure (lamellar units) and our model falls again short in that respect providing a simplified description of reality.

## 6 Conclusions

We conclude that in addition to collagen, arterial elastin plays an important role in anisotropic behavior of the tissue. The role of elastin, in anisotropic properties, is a result of its 3D structure, as observed by electron microscopy techniques, and affects the arterial mechanics mainly in the elastin-dominated region. Finally, elastin fragmentation appears to result in a later and less abrupt engagement of collagen fibers.

**Acknowledgments** The authors would like to thank Dr. Graham Knott and Stephanie Rosset at EPFL's SV Electron microscopy facilities for the assistance with specimen preparation and imaging, Alessandra Griffa and J. C. Sarria at EPFL's BIOP facilities for their assistance in image analysis and Dr. Bryn Martin for proofreading of the text. This work was supported by the Swiss National Science Foundation (Grant No. 325230-125445).

## References

Briggman KL, Denk W (2006) Towards neural circuit reconstruction with volume electron microscopy techniques. Curr Opin Neurobiol 16:562–570

Clark JM, Glagov S (1979) Structural integration of the arterial-wall .1. Relationships and attachments of medial smooth-muscle cells in normally distended and hyper-distended aortas. Lab. Invest. 40:587–602

Clark JM, Glagov S (1985) Transmural organization of the arterial media—the lamellar unit revisited. Arteriosclerosis 5:19–34

Daamen WF, Hafmans T, Veerkamp JH, Van Kuppevelt TH (2001) Comparison of five procedures for the purification of insoluble elastin. Biomaterials 22:1997–2005

Denk W, Horstmann H (2004) Serial block-face scanning electron microscopy to reconstruct three-dimensional tissue nanostructure. PLoS Biol 2:e329

Dingemans KP, Teeling P, Lagendijk JH, Becker AE (2000) Extracellular matrix of the human aortic media: an ultrastructural histochemical and immunohistochemical study of the adult aortic media. Anat Rec 258:1–14

Dobrin PB (1989) Patho-physiology and pathogenesis of aortic-aneurysms-current concepts. Surg Clin North Am 69:687–703

Dobrin PB, Canfield TR (1984) Elastase, collagenase, and the biaxial elastic properties of dog carotid-artery. Am J Physiol 247:H124–H131

Driessen NJB, Bouten CVC, Baaijens FPT (2005) A structural constitutive model for collagenous cardiovascular tissues incorporating the angular fiber distribution. J Biomech Eng-Trans Asme 127: 494–503

Driessen NJB, Bouten CVC, Baaijens FPT (2005) A structural constitutive model for collagenous cardiovascular tissues incorporating the angular fiber distribution. J Biomech Eng 127:494–503

Fonck E, Prod'hom G, Roy S, Augsburger L, Rufenacht D, Stergiopulos N (2007) Effect of elastin degredation on carotid wall mechanics as assessed by a constituent-based biomechanical model. Am J Physiol Heart Circ Physiol 292:H2754–H2763

Fung YC, Fronek K, Patitucci P (1979) Pseudoelasticity of arteries and the choice of its mathematical expression. Am J Physiol 237:H620–H631

Gasser TC, Ogden RW, Holzapfel GA (2006) Hyperelastic modelling of arterial layers with distributed collagen fibre orientations. J Royal Soc Interf 3:15–35

Grut W, Edwards J, Evans EJ (1977) Scanning electron microscopy of freeze-dried aortic elastin. J Microsc 110:271–275

Gundiah N, Ratcliffe BM, Pruitt AL (2007) Determination of strain energy function for arterial elastin: experiments using histology and mechanical tests. J Biomech 40:586–594

Gundiah N, Ratcliffe MB, Pruitt LA (2009) The biomechanics of arterial elastin. J Mech Behav Biomed Mater 2:288–296

Hayashi K, Takamizawa K, Nakamura T, Kato T, Tsushima N (1987) Effects of elastase on the stiffness and elastic properties of arterial-walls in cholesterol-fed rabbits. Atherosclerosis 66:259–267

Holzapfel GA, Gasser TC, Ogden RW (2000) A new constitutive framework for arterial wall mechanics and a comparative study of material models. J Elast 61:1–48

Holzapfel GA, Weizsacker HW (1998) Biomechanical behavior of the arterial wall and its numerical characterization. Comput Biol Med 28:377–392

Humphery JD (2002) Cardiovascular solid mechanics: cells, tissues and organs. Springer, New York

Lillie MA, Gosline JM (1990) The effects of hydration on the dynamic mechanical properties of elastin. Biopolymers 29:1147–1160

O'Connell MK, Murthy S, Phan S, Xu C, Buchanan J, Spilker R, Dalman RL, Zarins CK, Denk W, Taylor CA (2008) The three-dimensional micro- and nanostructure of the aortic medial lamellar unit measured using 3D confocal and electron microscopy imaging. Matrix Biol 27:171–181

Rezakhaniha R, Stergiopulos N (2008) A structural model of the venous wall considering elastin anisotropy. J Biomech Eng 130. doi:10.1115/1111.2907749

Roy S, Silacci P, Stergiopulos N (2005) Biomechanical proprieties of decellularized porcine common carotid arteries. Am J Physiol Heart Circ Physiol 289:H1567–H1576

Roy S, Tsamis A, Prod'hom G, Stergiopulos N (2008) On the in-series and in-parallel contribution of elastin assessed by a structure-based biomechanical model of the arterial wall. J Biomech 41:737–743

Silver FH, Snowhill PB, Foran DJ (2003) Mechanical behavior of vessel wall: a comparative study of aorta, vena cava, and carotid artery. Ann Biomed Eng 31:793–803

Treloar LRG (1942) Thermodynamic study of the elastic extension of rubber. Trans Faraday Soc 293–298

VanDijk AM, Wieringa PA, van der Meer M, Laird JD (1984) Mechanics of resting isolated single vascular smooth muscle cells from bovine coronary artery. Am J Physiol 246:C277–287

Vito RP, Dixon SA (2003) Blood vessel constitutive models-1995-2002. Ann Rev Biomed Eng 5:413–439

Watton PN, Ventikos Y, Holzapfel GA (2009) Modelling the mechanical response of elastin for arterial tissue. J Biomech 42:1320–1325

Zhou J, Fung YC (1997) The degree of nonlinearity and anisotropy of blood vessel elasticity. Proc Natl Acad Sci USA 94:14255–14260

Zulliger MA, Fridez P, Stergiopulos N, Hayashi K (2004a) A strain energy function for arteries accounting for wall composition and structure. J Biomech 37:989–1000

Zulliger MA, Stergiopulos N, Rachev A (2004b) A constitutive formulation of arterial mechanics including vascular smooth muscle tone. Am J Physiol Heart Circ Physiol 287:H1335–1343